Two distinct forms of functional lateralization in the human brain

Stephen J. Gotts[a,1], Hang Joon Jo[b,1,2], Gregory L. Wallace[a], Ziad S. Saad[b], Robert W. Cox[b], and Alex Martin[a]

[a]Section on Cognitive Neuropsychology, Laboratory of Brain and Cognition, and [b]Scientific and Statistical Computing Core, National Institute of Mental Health, National Institutes of Health, Bethesda, MD 20892

The hemispheric lateralization of certain faculties in the human brain has long been held to be beneficial for functioning. However, quantitative relationships between the degree of lateralization in particular brain regions and the level of functioning have yet to be established. Here we demonstrate that two distinct forms of functional lateralization are present in the left vs. the right cerebral hemisphere, with the left hemisphere showing a preference to interact more exclusively with itself, particularly for cortical regions involved in language and fine motor coordination. In contrast, right-hemisphere cortical regions involved in visuospatial and attentional processing interact in a more integrative fashion with both hemispheres. The degree of lateralization present in these distinct systems selectively predicted behavioral measures of verbal and visuospatial ability, providing direct evidence that lateralization is associated with enhanced cognitive ability.

specialization | asymmetry | intelligence | segregation | circuit

When considering the macroscopic functional organization of the human brain, it is a basic fact that particular capacities such as language, visuospatial attention, and hand preference in motor coordination are relatively lateralized to one of the two cerebral hemispheres (1, 2). Neuropsychological and neuroimaging studies have revealed a strong bias toward left-hemisphere representation of language and fine motor control of the hands (3, 4), with a well-documented association between handedness and language lateralization that is most pronounced in right-handed males (5). In contrast, visuospatial attentional abilities are represented more strongly in the right hemisphere, with right-sided brain damage being more likely to produce hemispatial attentional neglect (6). Although the mechanisms underlying functional lateralization are unknown, theoretical proposals have appealed to the computational benefits of functional specialization (7–9), with distinct functions and a division of labor between the hemispheres that improves overall cognitive ability and performance.

If functional lateralization is truly beneficial, a quantitative relationship should exist between the strength of lateralization and the level of cognitive ability. Indeed, relative hand skill, a behavioral marker of the lateralization of fine motor control, predicts verbal and nonverbal ability levels in both left- and right-handed individuals, with deficits observed in individuals with equal motor skills in the two hands (10). However, investigation of the brain bases of these relationships has been limited by several factors. A comprehensive evaluation of lateralization over the entire cortex requires establishing homotopic locations in the two hemispheres with high spatial precision, an alignment that is complicated by the presence of variable gyral folding patterns (11). Detailed hemispheric alignment methods by gyral and sulcal landmarks on the unfolded cortical surface have only recently been developed (12, 13). Previous neuroimaging studies of functional lateralization have also considered only one basic form of lateralization, quantified by comparing the overall magnitude or extent of task-engaged brain activity (14, 15) or the average strength of activity correlations in the left vs. the right

hemisphere (16, 17). A basic distinction that derives from the separate literatures on language, motor, and visuospatial lateralization is that the hemispheres differ qualitatively in their within- and between-hemisphere interactions (reviewed in ref. 18). Left hemisphere representations of language and fine motor control have been proposed to be more "focal," permitting rapid cortical interactions with shorter conduction delays (19–21), whereas right-lateralized visuospatial attention mechanisms require a greater degree of interhemispheric integration due to the bilateral representation of visual space (22). Nevertheless, the proposed preferences of each hemisphere for unilateral vs. bilateral interaction and how such preferences relate quantitatively to particular cognitive abilities have yet to be examined.

In the current study, we used functional (f)MRI to examine the hemispheric lateralization of time-varying cortico-cortical interactions in 62 right-handed male participants, and we evaluated the quantitative relationship of lateralization to behavioral measures of verbal and visuospatial ability. Rather than using a particular cognitive task during fMRI that would engage only a subset of relevant brain regions, we measured slow, spontaneous activity fluctuations present throughout the brain while participants were at rest (reviewed in ref. 23). Measures of verbal and visuospatial ability were then acquired outside the MRI scanner in a separate behavioral testing session. The lateralization of cortico-cortical interactions was determined by first identifying homotopic locations in the left and right hemispheres in terms of their anatomical positions relative to gyral and sulcal

Significance

This study alters our fundamental understanding of the functional interactions between the cerebral hemispheres of the human brain by establishing that the left and right hemispheres have qualitatively different biases in how they dynamically interact with one another. Left-hemisphere regions are biased to interact more strongly within the same hemisphere, whereas right-hemisphere regions interact more strongly with both hemispheres. These two different patterns of interaction are associated with left-lateralized functions, such as language and motor abilities, and right-lateralized functions, such as visuospatial attention. Importantly, the magnitude of lateralization measured for individual participants in these regions predicted the level of cognitive ability for the respective function, demonstrating that lateralization of function is associated with improved cognitive ability.

landmarks on the unfolded cortical surface (Fig. 1*A*). Resting brain activity at each location (36,002 nodes per hemisphere) was correlated with the activity at every other location within and across hemispheres, averaging these correlations separately per location to estimate the strength of intra- and interhemispheric cortical interactions (Fig. 1*B* and Fig. S1) (16, 24). Lateralization was then quantified at homotopic cortical locations, using two separate metrics that are differentially sensitive to a preference for within-hemisphere interactions ("segregation": within- minus between-hemisphere correlation) vs. between-hemisphere inter-

actions ("integration": within- plus between-hemisphere correlation), permitting the evaluation of these preferences throughout the entire cortex.

Results

Paired *t* tests applied separately to the segregation and integration metrics across participants [$P < 0.005$, corrected for false discovery rate (FDR) to $q < 0.025$ for both] revealed several large left-lateralized brain regions (Fig. 2 and Table S1). Although a few smaller regions revealed significant left lateralization for the
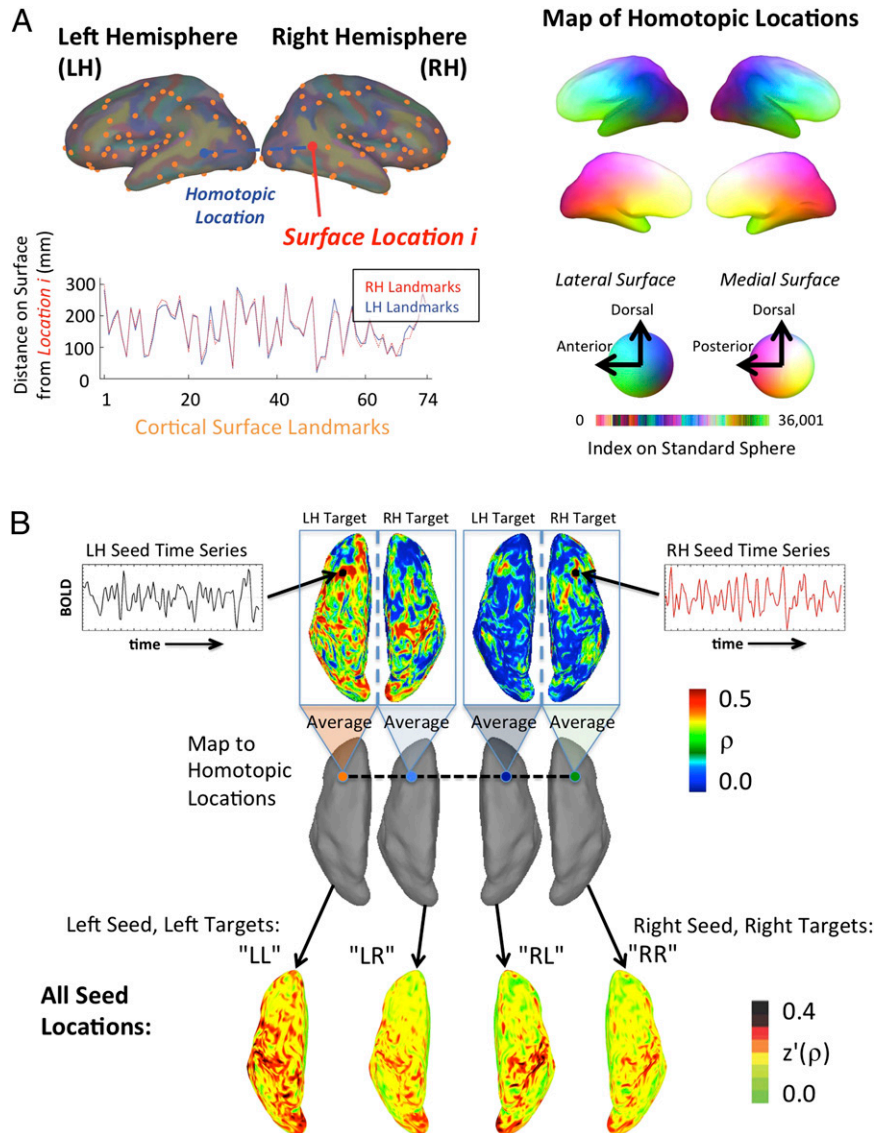

Fig. 1. Comparing within- and between-hemisphere cortical interactions at homotopic locations. (*A*) Homotopic locations in the two hemispheres were identified using relative position on the cortical surface from the centroids of FreeSurfer's automatically parcellated regions, with 74 regions in each hemisphere delimited by gyral and sulcul boundaries. (*Upper Left*) The locations of the centroids are shown on the cortical surfaces (small orange circles), and the process of mapping the homotopic location (in blue) of a surface location *i* in the right hemisphere (in red) is graphically depicted. The homotopic location is the surface node (of 36,002) in the opposite hemisphere with the most similar pattern of distances (geodesic) to the original node (see red and blue traces, *Lower Left*). (*Right*) A complete map of homotopic locations for the standard surface model is shown, using color (see key for color map of locations). (*B*) After identifying homotopic locations, the average within- and between-hemisphere correlation coefficient (*ρ*) was calculated using resting brain activity at each node and compared at homotopic locations. (*Top*) Two homotopic seed nodes and their Blood-Oxygenation-Level-Dependent, or BOLD, time series, one in the left hemisphere (LH) and one in the right (RH), along with their corresponding correlation maps in the LH and RH targets (color bar, *Right*). The correlation maps in the target hemispheres are then averaged over the entire hemisphere (*Middle*) and stored back at the seed location, separately for the within- and between-hemisphere correlations. (*Bottom*) The results of this process when repeating for all seed locations, applying Fisher's z′-transform to yield normally distributed values, and then averaging across all participants on the standard cortical surface (color bar, *Right*). The first letter in the labels "LL," "LR," "RR," and "RL" indicates a seed location in the left (L) or right (R) hemisphere, and the second letter indicates the target hemisphere (Fig. S1).

www.manaraa.com

integration metric, the left-lateralized locations were dominated by the results for the segregation metric, reflecting a tendency for stronger intrahemispheric correlations on the left, along with weaker correlations from left to right (Fig. S1). These locations included left-hemisphere language areas such as the left inferior frontal gyrus; the posterior and middle superior temporal and middle temporal gyri (25); brain regions involved in social processing and communication such as the posterior cingulate, medial frontal, and ventral temporal cortex including the fusiform gyrus (26); and portions of the left somatosensory and motor cortex involved in motor coordination of the arms, hands, and mouth (27); as well as medial occipital regions near the calcarine sulcus. In contrast, virtually all right-lateralized regions were observed solely with the integration metric, indicating stronger intra- and interhemispheric correlations with locations on the right. These consisted of brain regions involved in visuospatial and attentional processing such as the right superior parietal cortex, occipital cortex, and regions in ventral temporal cortex, including the fusiform and parahippocampal gyri (22, 28). When comparing the magnitudes of segregation and integration statistically (paired t tests) for the regions shown in Fig. 2, greater lateralization was detected for the segregation metric in the left somatosensory/motor cortex [$t = 3.44$, $n = 62$, $P < 0.001$], the left anterolateral temporal [$t = 7.14$, $n = 62$, $P < 0.0001$] and ventral temporal cortex [$t = 8.05$, $n = 62$, $P < 0.0001$], and the left posterior cingulate [$t = 2.25$, $n = 62$, $P < 0.03$] and medial frontal cortex [$t = 2.13$, $n = 62$, $P < 0.04$], as well as the medial occipital cortex superior to the calcarine sulcus [$t = 6.25$, $n = 62$, $P < 0.0001$]. In contrast, greater lateralization for the integration metric was observed for all of the right-hemisphere regions shown in Fig. 2 that were identified with the integration metric [$t > 6.75$, $n = 62$, $P < 0.0001$ for all]. These results establish the presence of two qualitatively different forms of lateralization that are associated with the two cerebral hemispheres, with the left hemisphere exhibiting cortico-cortical interactions that are constrained toward the left hemisphere and the right hemisphere exhibiting interactions that are strongly bilateral.

Interrelationships of Lateralized Brain Regions. We next examined the interrelationships of the 10 left-lateralized regions detected with the segregation metric and the 8 right-lateralized regions detected with the integration metric. Multidimensional scaling and cluster analyses were used to identify sets or collections of regions that had similar patterns of correlation with the others, highlighting regions that are likely to belong to a common processing circuit (Fig. 3). Given the large differences in surface area of these regions, correlations of resting brain activity were calculated among a fixed number of individual surface locations, randomly sampled from the larger regions of interest. These locations were then clustered with the K-means algorithm, and this process was repeated 100 times to determine the average likelihood that locations from any pair of regions were clustered together. Estimates of the chance likelihood of clustering were determined in Monte Carlo simulations by applying the same clustering methods to random data (*Methods* and Fig. S3). The average likelihood region-by-region matrix was then submitted to multidimensional scaling (Fig. 3A) and a final round of clustering to determine which regions have the most similar patterns of correlation with respect to the other regions. A four-cluster solution provided the best trade-off of variance explained to model complexity (Fig. 3A, *Inset*), with clusters coded by color and labeled 1–4. The left-hemisphere language regions clustered together with those involved in other aspects of social processing and communication (Fig. 3 B and C, shown in red for cluster 1); the left somatosensory/motor regions involved in the coordination of arm, hand, and mouth movements clustered together with ventral temporal regions that are active when viewing, naming, and thinking about manipulable objects (29) (outlined in green
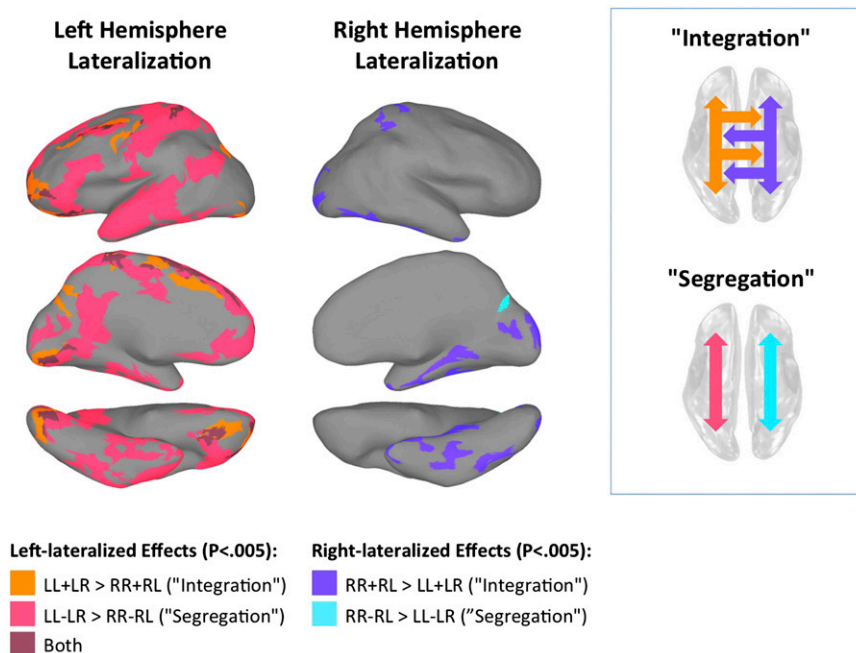

Fig. 2. Correlations in resting brain activity are lateralized to the left vs. right hemispheres in a qualitatively distinct manner. (*Left*) Regions detected with the "segregation" metric exhibited a relative shift toward stronger within- relative to across-hemisphere correlations. (*Center*) Regions detected with the "integration" metric exhibited a shift toward stronger summed within- and across-hemisphere correlations. Metrics were compared at homotopic locations in the left and right hemispheres. For each surface location (node), integration = LL + LR − (RR + RL) and segregation = LL − LR − (RR − RL), with positive (negative) sign indicating left (right) lateralization. Label conventions are the same as in Fig. 1. See Fig. S2 for display of the same results in more typical views on the folded cortical surface.
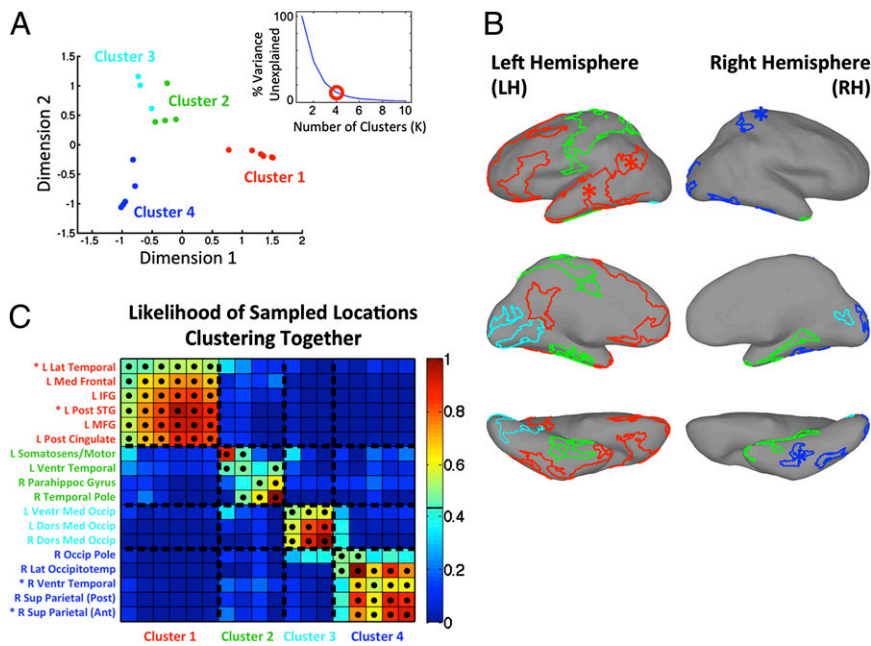
Gotts et al.

Fig. 3. Activity correlations among lateralized brain regions form four function-related clusters. Locations were randomly sampled from each region, the resulting correlation matrix was clustered, and the average likelihood that sampled locations were clustered together was calculated. (*A*) Agreement of multidimensional scaling and K-means clustering of the average likelihood matrix, along with an "elbow" plot of variance left unexplained relative to the number of clusters, indicate four distinct clusters (clusters 1–4), shown using color (red, green, and light and dark blue). (*B*) Viewing the anatomical locations of clusters on the cortical surface reveals that the red regions (cluster 1) correspond to left-hemisphere regions involved in language and social communication; the green regions correspond to somatosensor, motor, and ventral temporal regions (cluster 2); the light blue regions correspond to medial occipital regions engaged in early stages of vision (cluster 3); and the dark blue regions correspond to right-hemisphere regions involved in higher-level aspects of visuospatial processing (cluster 4). (*C*) Good internal consistency of the four clusters is observed when viewing the average likelihood matrix used in *A*, sorted by cluster membership. (*Right*) Color bar indicates the probability that randomly sampled locations from the regions cluster together over 100 iterations. Labels corresponding to each of the 18 lateralized regions are provided next to the rows of the matrix in *C*. Solid black circles in the cells of the matrix in *C* indicate that the cluster likelihood exceeds the level expected due to chance (Bonferroni corrected to $P < 0.05$ for the number of unique comparisons in the 18×18 matrix). Asterisks (*) next to the labels in *C* and placed in the interior of the regions in *B* highlight regions that exhibit behavioral correlations in Figs. 4 and 5. (Abbreviations: Ant, anterior; Dors, dorsal; IFG, inferior frontal gyrus; L, left; Lat, lateral; Med, medial; MFG, middle frontal gyrus; Occip, occipital; Occipitotemp, occipitotemporal; Parahippoc, parahippocampal; Post, posterior; R, right; Somatosens, somatosensory; STG, superior temporal gyrus; Sup, superior; Ventr, ventral.)

for cluster 2); and the early visual and high-level visuospatial regions formed two separate clusters, one composed of bilateral medial occipital regions and the other of right-lateralized occipital, lateral ventral temporal, and parietal regions (outlined in light and dark blue, respectively, for clusters 3 and 4). When controlling for the chance level of clustering (Bonferroni corrected to $P < 0.05$), all of the regions were significantly clustered together in clusters 1 and 3 (shown as black circles in Fig. 3*C*), and all of the regions in cluster 4 were significantly clustered together with the exception of the right occipital pole region, which was clustered significantly only with the right lateral occipitotemporal region. The left somatosensory/motor region in cluster 2 was clustered together significantly only with the left ventral temporal region, failing to cluster significantly with the other two regions in cluster 2. Taken together, these analyses indicate that the 18 lateralized regions are not uniformly related to one another. Rather, they are organized coarsely into a smaller number of functionally related groups, with regions associated previously with aspects of language and high-level visuospatial functions clustering together in clusters 1 and 4, respectively.

Relationship of Lateralization to Verbal and Visuospatial Ability. Having identified the large-scale organization of these lateralized brain regions, it was possible to ask how well the magnitude of lateralization in regions involved in language and visuospatial processing could predict the corresponding cognitive abilities. A subset of 44 participants was administered the Wechsler Abbreviated Scale of Intelligence (WASI), which includes vocabulary and block design subtests shown to correlate more broadly with language and visuospatial abilities, respectively (30–33). Vocabulary and block design scores were found to be moderately intercorrelated in this participant sample ($r = 0.309$, $P < 0.05$). Therefore, we used standard and partial correlation methods to separate out the unique portions of variation in each measure that were associated with the two lateralization metrics. We also constrained our analyses to the two sets of brain regions identified in the cluster analyses that were most directly relevant, cluster 1 regions associated with language and social communication and cluster 4 regions associated with high-level visuospatial processing. We first evaluated the relationship between the magnitude of lateralization (segregation) in the six identified cluster 1 regions and the vocabulary score. Of these six regions, only the three regions that are most strongly associated with language function (25) showed a significant positive correlation between the segregation metric and the vocabulary score (left inferior frontal gyrus, $r = 0.303$, $n = 44$, $P < 0.05$, two-tailed; left lateral temporal cortex, including the superior, middle, and inferior temporal gyri, $r = 0.348$, $n = 44$, $P < 0.03$; and the posterior superior temporal gyrus, $r = 0.376$, $n = 44$, $P < 0.02$). After partialling out the shared variation with block design scores to establish selectivity to verbal ability, a positive partial correlation with the vocabulary score remained for the left lateral temporal region (*partial r* $= 0.340$, $n = 44$, $P < 0.03$) and the left posterior superior temporal region (*partial r* $= 0.400$, $n = 44$, $P < 0.01$) (Fig. 4, *Left*). Only the segregation metric was found to
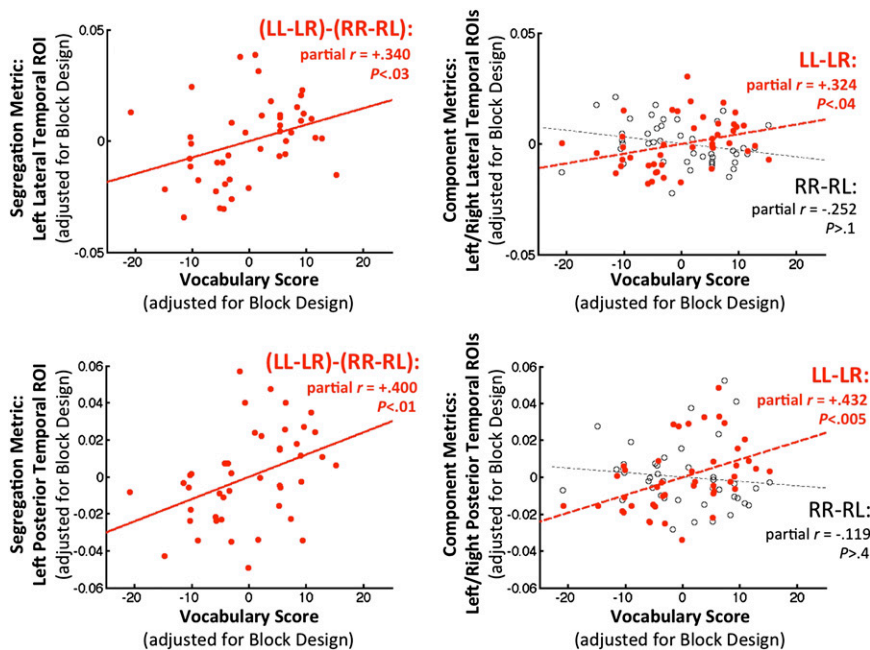
Fig. 4. Magnitude of lateralization in lateral temporal regions predicts verbal ability levels. The Segregation metric in the left lateral temporal cortex (*Upper*) is correlated with the vocabulary score after partialling the block design score across participants. The scatterplot for the full segregation metric [(LL−LR)−(RR−RL)] is shown to the left, adjusting both axes for the block design score. The same scatterplot is shown to the right, broken down by the corresponding left-hemisphere (LL−LR) and right-hemisphere components (RR−RL) of the full metric. (*Lower*) Analogous results are shown for the posterior temporal region. Label conventions are the same as for Fig. 1. Compare with whole-brain partial correlation results for individual surface locations shown in Fig. S4.

be associated with the vocabulary score in these regions; correlations and partial correlations calculated for the integration metric using these same regions failed to yield significant results ($P > 0.2$ for all). However, because correlations involving the segregation metric intrinsically involved a comparison of homotopic locations in the left and right hemispheres, it was important to examine whether the cortico-cortical interactions with the left-hemisphere regions were more responsible for the results than those with the right. Significant partial correlations with the vocabulary score of left-with-left hemisphere minus left-with-right hemisphere activity correlations (labeled as "LL-LR" in Fig. 4, *Right*) were found for both the left lateral temporal (*partial r* = 0.324, $n = 44$, $P < 0.04$) and the left posterior superior temporal regions (*partial r* = 0.432, $n = 44$, $P < 0.005$). No significant relationships were observed for the homotopic right-hemisphere contrasts ("RR-RL" in Fig. 4, *Right*). In summary, the magnitude of lateralization in two cluster 1 regions was selectively associated with better vocabulary scores, but only when examining the lateralization metric appropriate for these regions (i.e., segregation).

We similarly examined the magnitude of lateralization in the five identified right-hemisphere cluster 4 regions that are most strongly associated with high-level visuospatial processing and correlated these values with block design scores, partialling out common sources of variation with the vocabulary score. We observed a significant partial correlation between the integration metric and the block design score in a large region of ventral temporal cortex, spanning portions of the fusiform gyrus, the anterior transverse collateral sulcus, and the inferior temporal gyrus (*partial r* = 0.398, $n = 44$, $P < 0.01$) (Fig. 5*A*, *Left*), along with a nonsignificant trend in one of the two right superior parietal regions (*partial r* = 0.255, $n = 44$, $P < 0.1$). As with the previous results, the partial correlation in right ventral temporal cortex was not obtained when using the opposite lateralization metric (segregation: $P > 0.4$), and it was driven by the right-hemisphere portions of the integration metric (RR+RL: *partial r* = 0.349, $n = 44$, $P < 0.03$) (Fig. 5*A*, *Right*), with no relationship observed using the homotopic left-hemisphere region (LL+LR: *partial r* = 0.067, $n = 44$, $P > 0.6$). However, multiple tests were conducted on visuospatial regions (five in all), raising the possibility that these results might be due to α-inflation from

multiple comparisons. We therefore examined independent behavioral data from an additional subtest on the WASI that also indexes visuospatial processing abilities, along with more abstract reasoning abilities: the matrix reasoning subtest (*Methods*). As with the results for block design, the right ventral temporal region showed a significant partial correlation between the integration metric and the matrix reasoning score after partialling out the vocabulary score (*partial r* = 0.355, $n = 44$, $P < 0.02$) (Fig. 5*B*, *Upper Left*), along with a significant partial correlation in the right parietal region that previously showed a trend-level association for the block design score (*partial r* = 0.353, $n = 44$, $P < 0.03$) (Fig. 5*B*, *Lower Left*). Results were not obtained in either region when using the segregation metric ($P > 0.4$ for all), and they were similarly driven by the right-hemisphere portions of the integration metric in the ventral temporal region (matrix reasoning, RR+RL, *partial r* = 0.432, $n = 44$, $P < 0.005$; LL+LR, $P > 0.19$) (Fig. 5*B*, *Upper Right*), as well as in the right parietal region (matrix reasoning, RR+RL, *partial r* = 0.333, $n = 44$, $P < 0.03$; LL+LR, $P > 0.7$) (Fig. 5*B*, *Lower Right*), replicating the overall pattern observed with block design scores.

The common pattern observed across this series of region-of-interest (ROI) tests was highly replicable: (*i*) significant partial correlation with the metric used to identify the lateralized region, (*ii*) the lack of a significant partial correlation with the opposite metric ($P > 0.1$), (*iii*) a significant partial correlation with the same-sided component of the full laterality metric, and (*iv*) the lack of a significant partial correlation with the opposite-sided component metric ($P > 0.1$). These observations strongly suggest that the observed behavioral correlations are not due to chance. Although straightforward calculation of the joint likelihood of all of these events for each ROI is not possible (the comparisons are not orthogonal), it is possible to estimate their joint likelihood when using random permutations of the same data (34). The process involves randomly repairing each participant's laterality measures with another participant's behavioral scores, recalculating all of the same partial correlations on the randomized data, and then repeating this process many times (20,000 iterations used in the current study; see *Methods* for full details), counting the number of times that the joint events occur due to chance. When applying this procedure to the current data, the joint pattern of events was found to be exceedingly unlikely
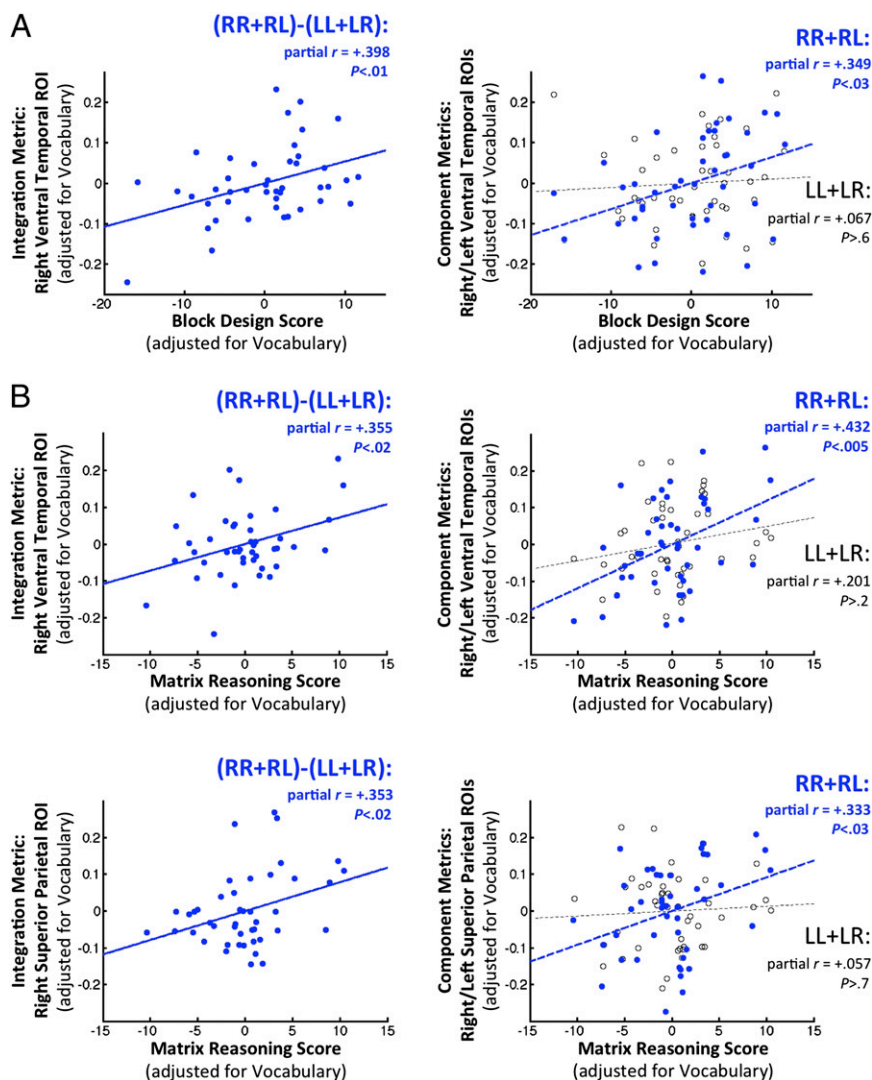
A

(RR+RL)−(LL+LR):
partial r = +.398
P<.01

RR+RL:
partial r = +.349
P<.03

LL+LR:
partial r = +.067
P>.6

B

(RR+RL)−(LL+LR):
partial r = +.355
P<.02

RR+RL:
partial r = +.432
P<.005

LL+LR:
partial r = +.201
P>.2

(RR+RL)−(LL+LR):
partial r = +.353
P<.02

RR+RL:
partial r = +.333
P<.03

LL+LR:
partial r = +.057
P>.7

Fig. 5. Magnitude of lateralization in ventral temporal and superior parietal regions predicts visuospatial ability levels. (*A*) The Integration metric in the right ventral temporal cortex is correlated with block design scores after partialling vocabulary scores across participants. (*Left* and *Right*) The adjusted scatterplot for the full Integration metric is shown [(RR + RL) − (LL + LR)] (*Left*) and broken down by right- and left-hemisphere components (*Right*). Similar results at a trend level (*P* < 0.1) were obtained for the right superior parietal region (main text). (*B*) The integration metric in the right ventral temporal and superior parietal regions is correlated with matrix reasoning scores after partialling vocabulary scores across participants. Scatterplot conventions are as in *A*. Label conventions are the same as for Fig. 1. Compare with whole-brain partial correlation results for individual surface locations shown in Fig. S4.

for each ROI reported in Figs. 4 and 5 (left lateral temporal ROI, $P < 0.0027$; left posterior superior temporal ROI, $P < 0.0007$; right ventral temporal ROI for block design, $P < 0.0016$; right ventral temporal ROI for matrix reasoning, $P < 0.0016$; right superior parietal ROI for matrix reasoning, $P < 0.0024$). Although no single test would survive Bonferroni correction for the number of regions tested in these analyses (16 total: 6 for cluster 1 ROIs and 5 for cluster 4 ROIs, each tested twice), the joint likelihood of the full pattern of results for each ROI did survive correction ($P < 0.05/16 = 0.003125$), establishing that the observed patterns of results are not due to chance.

Lateralization in Language-Related Regions Predicts Lateralization in Motor-Related Regions but Is Distinct from Lateralization in Visuospatial Regions. We have demonstrated that for multiple brain regions involved in the domains of both language and visuospatial processing, the magnitude of lateralization is positively associated with the level of cognitive ability. However, the presence of significant partial correlations does not rule out the possibility of at least a portion of shared variation between verbal and visuospatial domains. Indeed, the "functional crowding" hypothesis of brain lateralization holds that as one function becomes lateralized, such as fine motor control or language, it forces the lateralization of other functions as all of them compete for cortical representation (35). Recent fMRI evidence

(36) suggests that for left-handed participants with and without atypical speech lateralization, measures of verbal and visuospatial lateralization are indeed interrelated (15). However, the same issue has not been evaluated in a whole-brain manner across verbal, visuospatial, and motor domains in more typical right-handed participants. Accordingly, we examined the extent to which it is possible to predict the magnitude of lateralization in one functional domain, using the magnitude derived from another. For these purposes, we focused not only on regions in clusters 1 and 4, but also on regions in cluster 2 related to motor coordination (the red, dark blue, and green clusters in Fig. 3). We controlled for the potential concern that global correlations across the entire spatial extent of the brain could bias the interrelatedness of these lateralization measures by partialling out the level of whole-brain correlation present for each participant from the lateralization metrics in each region (*Methods*). Averaging the resulting adjusted lateralization metrics across regions within each cluster, the magnitude of lateralization in cluster 1 regions strongly predicted the magnitude of lateralization in cluster 2 regions across participants ($r = 0.606$, $n = 62$, $P < 0.0001$). In contrast, neither the cluster 1 nor the cluster 2 regions predicted the magnitude of lateralization in cluster 4 regions associated with high-level visuospatial processing ($r = 0.073$, $n = 62$, $P > 0.5$ and $r = 0.077$, $n = 62$, $P > 0.5$, respectively). Both of these correlations were near zero, and they were

www.manaraa.com

also significantly below the level of correlation observed between lateralization magnitudes in clusters 1 and 2 (using Fisher's z-transform to test for significant differences in two correlation coefficients: $r = 0.606$ vs. 0.073, $n = 62$, $P < 0.001$; $r = 0.606$ vs. 0.077, $n = 62$, $P < 0.001$). In contrast to the recent results of Cai et al. (36), these results fail to support the functional crowding hypothesis for typical right-handed participants. Instead, they provide evidence for independent mechanisms of functional lateralization in the left vs. right hemispheres (see ref. 37 for similar evidence from transcranial Doppler imaging).

Discussion

Using two different metrics to detect the hemispheric lateralization of cortico-cortical interactions in resting brain activity, we have demonstrated that the left hemisphere has a greater preference for within-hemisphere interactions whereas the right hemisphere has interactions that are more strongly bilateral. At a macroscopic scale, this is broadly consistent with proposals that hold that cortical representations are more focal in the left hemisphere and more diffuse in the right hemisphere (21). We have also demonstrated that hemispheric lateralization of verbal and visuospatial function is quantitatively beneficial for these functions when examining the appropriate lateralization metrics, at least within the population of right-handed males on which much of the laterality literature has been based (38). Although we were unable in the current study to evaluate the quantitative relationship between fine motor skill and the magnitude of lateralization in the left somatosensory and motor cortex, our results afford the strong prediction that performance in speeded manual and/or pronunciation tasks should be directly related to the segregation metric calculated for this part of the brain.

Cluster analyses identified four sets of lateralized brain regions that interact differentially with one another. In cluster 1, classic language regions in the left inferior frontal and lateral temporal cortex were grouped together along with regions in the same hemisphere on the medial wall that are associated with social communication and comprehension (16, 25, 26, 39, 40). In cluster 2, somatosensory and motor regions responsible for the control of the arms, hands, and mouth were significantly grouped with a left medial ventral temporal region (Fig. 3C and Fig. S5) that is more active when performing cognitive tasks with manipulable objects than with stimuli from animate categories (29). This finding is consistent with recent anatomical evidence of a distinct pathway from parietal to ventromedial temporal cortex that may be involved in visually guided reaching and grasping of objects (41). The further involvement of the portion of the motor cortex responsible for controlling the mouth and tongue for speech suggests a larger designation of brain regions involved in fine motor coordination (see Fig. S6 for comparison of localization in prior studies; e.g., refs. 27, 42). Although language and motor coordination of the limbs are clearly distinct functions, the magnitude of lateralization measured from the corresponding brain regions was found to be tightly interrelated across participants, consistent with the well-known relationship between handedness and language lateralization (5, 38). The fact that these left-hemisphere regions were all identified with the segregation metric, indicating interactions that are predominantly restricted to the left hemisphere, concords well with previous proposals that more spatially restricted, focal cortical representations could be beneficial for systems that require temporally rapid interactions in the service of sequential behaviors (19–21).

The remaining two clusters of brain regions (clusters 3 and 4) were associated with aspects of visuospatial function. Medial occipital areas involved in early vision formed one cluster, and higher-level occipital, ventral temporal, and superior parietal areas involved in more complex aspects visuospatial processing and attention formed the other. Although some studies have found evidence supporting an interdependence of lateralization

in visuospatial and language processing (e.g., ref. 36), the magnitude of lateralization in right-hemisphere visuospatial brain regions in our large sample of right-handed male participants was found to be independent of lateralization magnitude in left-hemisphere language and motor regions. This finding suggests that separate genetic and/or neural mechanisms are responsible for driving lateralization in the two hemispheres. The differences between the results of ref. 36 and our current study may reflect differences in the participant samples (e.g., the inclusion of left-handed participants) or perhaps in the methods used to assess lateralization (cortico-cortical interactions measured in resting brain activity vs. the magnitude of task-evoked responses in particular brain regions). Indeed, it will be important for future studies to examine the agreement of laterality measures taken during the performance of explicit tasks vs. those taken at rest, as in the current study. It is possible that some aspects of our current results are invariant across task conditions, whereas others may vary in a more context-sensitive manner. Task-evoked responses and patterns of covariation of resting-brain activity are both thought to depend on the underlying structure of synaptic connections (43, 44), but particular tasks may engage certain synaptic connections differentially. We would expect task conditions that critically rely on regions discovered using our resting-state methods to yield comparable lateralization results and correspondences with behavior. Nevertheless, it is noteworthy that measures of lateralized cortical interactions taken during rest can be associated with individual variability in behavioral measures that were acquired in a separate session, implying that an ample portion of this variability is context invariant. In principle, the presence of these sorts of brain–behavior relationships when using resting brain activity should afford comparative studies throughout development, as well as across different species, that would otherwise be difficult or impossible to conduct due to a lack of task competence in certain populations (45, 46).

Although our current results do not highlight interrelationships across verbal and visuospatial cognitive domains, the abundance of data from different methods points to there being a substantial portion of variation that is shared across these domains. For example, Crow et al. (10) examined interrelationships between behavioral measures of verbal and nonverbal ability (e.g., detecting patterns in a series of visual shapes) in more than 12,000 right- vs. left-handed participants. Strong direct relationships were observed between verbal and nonverbal performance across participants, as well as a dependence of performance in each domain on relative hand skill. Similarly, the literature on "g," a single factor of general intelligence, commonly finds robust intercorrelations of test performance across verbal and nonverbal subtests of the Wechsler scales and other Intelligence Quotient (IQ) tests (see ref. 47 for review). In our own participant sample, the correlation between vocabulary and block design scores was moderately positive and significant ($r = 0.309$, $P < 0.05$). In the context of this larger literature, our results do not imply a complete independence of verbal and nonverbal abilities, but rather a partial independence, with substantial portions of both shared and distinct variability (33, 48–50).

Our results are broadly consistent with computational theories of functional specialization that hold that information processing is more effective and efficient when larger functions can be decomposed into smaller independent processes, reducing functional interference (7, 8). Hemispheric lateralization can be thought of as a special case of functional specialization, but other cases, such as the division of labor in the visual system between space and form (41, 51) or category selectivity in occipito-temporal brain regions (29), may ultimately be found to follow similar considerations. In this regard, it is important to emphasize that although qualitatively different patterns of lateralized cortical interactions in the left and right hemispheres were ob-

Gotts et al.

served in the current study, these differences were nevertheless graded in nature, varying quantitatively over participants. We interpret this variation as being consistent with a developmental bias in synaptic connectivity and/or plasticity mechanisms that varies qualitatively by hemisphere and is optimized through experience (9). On this view, functions with a strong reliance on rapid, sequential interactions, such as speech production and comprehension (52) and fine motor control, may come to be represented in the left hemisphere by virtue of the bias toward intrahemispheric interactions with shorter average synaptic delays. In contrast, visuospatial processing that depends more prominently on information representation in space rather than in time may benefit more from the spatial conjunction of many synaptic inputs from both hemispheres, better matching the bias of the right hemisphere. This view is not only consistent with the data and proposal of Semmes for focal representations in the left hemisphere and more diffuse representations in the right hemisphere (21), but also consistent with a recent magnetoencephalography (MEG) study by Gazzaniga and coworkers showing stronger bilateral dynamical interactions when presenting words and pronounceable nonwords to the right hemisphere than when presenting these stimuli to the left hemisphere (53). With further developmental studies from infants through adulthood, we should be able to clarify at what point hemispheric differences in cortico-cortical interactions emerge, as well as to what extent these differences predict the acquisition of lateralized cognitive abilities.

Methods

Participants. Sixty-two right-handed males (mean age = 21.2 y, SD = 5.1 y) with no history of psychiatric or neurological disorders participated in the experiment. All had normal or corrected-to-normal vision. Handedness for a variety of activities, including writing, was confirmed through the administration of the Physical and Neurological Examination for Soft Signs (54). Informed assent and consent were obtained from all participants and/or their parent/guardian (participants younger than 18). The experiment was approved by the Institutional Review Board of the National Institutes of Health.

Behavioral Methods. The WASI (55) was administered to a subset of 44 of the 62 participants in a testing session that was separate from the MRI scanning session (all within 1 y of the scanning session). Individual t-scores (normative mean = 50, SD = 10) were available for each individual on four subtests, two contributing to estimates of verbal ability (Verbal IQ) (vocabulary, similarities) and two contributing to estimates of nonverbal ability (Performance IQ) (block design, matrix reasoning). From these, vocabulary and block design subtests were selected a priori for two main reasons: (*i*) Vocabulary and block design subtests have a long history of validity (56) and strong prior and selective associations with verbal/language abilities and visuospatial abilities, respectively (30–33, 47, 57, 58), and (*ii*) similarities and matrix reasoning both require more abstract reasoning, with the expectation that variation in scores will be driven relatively more by variation in domain-general executive functioning rather than the selective, lateralized abilities that are the focus of the current study. Furthermore, neuropsychological studies have established that left- vs. right-hemisphere damage has dissociable effects on vocabulary and block design scores (33), with these two subtests (along with digit span) also exhibiting the most robust brain–behavior correlations of those Wechsler subtests that have been examined to date in neuroimaging studies (57–59).

fMRI Imaging Methods. fMRI data were collected using a GE 3 Tesla whole-body MRI scanner at the National Institutes of Health Clinical Center NMR Research Facility, using standard imaging procedures. For each participant, a high-resolution T₁-weighted anatomical image (magnetization-prepared rapid acquisition with gradient echo, or MPRAGE) was obtained (124 axial slices, 1.2-mm slice thickness, field of view = 24 cm, 224 × 224 acquisition matrix). Spontaneous, slowly fluctuating brain activity was measured during fMRI, using a gradient-echo echo-planar imaging (EPI) series with whole-brain coverage while participants maintained fixation on a central cross and were instructed to lie still and rest quietly (repetition time, TR = 3,500 ms, echo time, TE = 27 ms, flip angle = 90°, 42 axial contiguous interleaved slices per volume, 3.0-mm slice thickness, field of view, FOV = 22 cm, 128 × 128 acquisition matrix, single-voxel volume = 1.7 × 1.7 × 3.0 mm). Each resting scan

lasted 8 min 10 s for a total of 140 consecutive whole-brain volumes. All EPI data were evaluated for sharp head motion artifacts, passing the sudden motion detection of the Analysis of Functional NeuroImages, or AFNI, program "afni_proc.py" at the threshold level 0.3 mm for the Euclidean L2 norm of motion displacement during each TR interval (60). Independent measures of nuisance physiological variables (cardiac and respiration) were recorded during the resting scan for later removal. A GE eight-channel send–receive head coil was used for all scans, with a sensitivity encoding for fast MRI, or SENSE, factor of 2 used to reduce gradient coil heating during the session.

fMRI Preprocessing. AFNI cross-modal registration software was used to align anatomical images for each participant to the fifth volume of the resting EPI time series. Aligned anatomical images were then processed with FreeSurfer's automated pipeline for generating cortical surface models and whole brain segmentation (61). The following procedures were carried out using AFNI's suite of programs (62). For each participant, standard-mesh surfaces of 36,002 nodes per hemisphere were created with AFNI Surface Mapper, or SUMA. A similar process was applied to the N27 template brain, allowing the display of the results onto the template's surfaces (63, 64). Preprocessing of the resting EPI time series was carried out using the basic anatomy-based image correction, or ANATICOR, method (65). The first four pre–steady-state TRs were removed. Large transients were transformed to lie between 2.5 and 4 SD from a smoothed version of the time series (AFNI's 3dDespike). Time series volumes were registered to the first volume of the truncated set and corrected for slice-time acquisition. Linear regression was used to remove motion, cardiac, respiratory, and hardware-induced signal transients. Respiration and aliased cardiac signals were created from the recorded physiological traces, using the retrospective image correction, or RETROICOR, approach (66). Additionally, five respiration-volume per-time (RVT) regressors (67) were added to model slow fluctuations in participant breathing patterns. Motion effects were modeled by the six head motion estimates, and hardware artifacts were modeled with one regressor for eroded local white matter signals and one averaged signal from eroded lateral ventricle masks. With the exception of the RVT regressors (which already include signals interpolated at five different time delays), 1-TR delayed versions of the nuisance variables were also included to allow for delayed effects of noise sources (68). The denoised, volume-based residual time series (length = 136 TRs) were then mapped onto cortical surfaces, using an average kernel with 10 sampling points evenly distributed along a line centered between smooth white matter and pial surfaces and extending 80% of the thickness between corresponding nodes on the two surfaces. The mapped time series were smoothed with a heat kernel that resulted in an 8 mm full-width-at-half-maximum noise spatial correlation structure on the white matter surface (12).

Finding Homotopic Locations Through Landmark-Based Correspondence. Homotopic locations in the two hemispheres were identified relative to gyral and sulcal landmarks on the cortical surface as in Jo et al. (12). We assigned to each cortical node a 74-dimensional label vector containing the geodesic distance along the surface from that node to each centroid of the 74 cortical parcellations provided by FreeSurfer (e.g., central sulcus, inferior frontal gyrus, etc.) to redefine locations on the cortical surfaces instead of the Cartesian coordinate system (x, y, z),

$$\vec{n} \equiv \langle \delta_1, \delta_2, \cdots, \delta_{74} \rangle,$$

where $\vec{n}$ is the label vector to define the position of a node in the hemisphere, and δ_j is the geodesic distance (46) between the node and the centroid of the jth FreeSurfer cortical parcellation, which is calculated on the standardized smooth white matter surfaces by SUMA's SurfDist program. The homotopic location of a cortical node can be defined as the node in the opposite hemisphere whose label vector is most similar to (i.e., has the largest Pearson correlation with) the original node's label vector (Fig. 1*A*).

Measuring Lateralized Cortical Interactions Using Within- and Across-Hemisphere Average Correlation. As in previous studies of "functional connectivity" using resting brain activity (23), the strength of cortical interactions between two locations on the cortical surface was estimated as the correlation (Pearson's r) of the residual EPI time series at those locations. Taking each individual surface node as a "seed," the correlation of the corresponding resting time series was calculated with every other surface node in both hemispheres as "targets". These correlations were then averaged within and across hemisphere for each seed node, estimating the average strength of intra- and interhemispheric interactions with the seed location (Fig. 1*B*) (16, 24). After applying Fisher's z-transform to these averaged correlations to yield normally distributed values,

www.manaraa.com

within- and across-hemisphere contrasts were calculated for each participant between homotopic locations in the left and right hemispheres to estimate two different forms of functional lateralization. Segregation, the tendency for greater within- relative to across-hemisphere interactions, was calculated as

$$Segregation = LL - LR - (RR - RL).$$

The first letter in these labels denotes the seed hemisphere and the second denotes the target hemisphere (e.g., "LR" means the average correlation of a seed node in the left hemisphere with all target surface nodes in the right hemisphere). A large positive value of $LL-LR$ would indicate that the average correlation within the left hemisphere was stronger than the average correlation from the left to the right hemisphere. A large positive value of the full segregation metric would indicate that the bias for stronger within-hemisphere interactions is stronger for the left than for the right hemisphere. In contrast, a large negative value would indicate that the bias for within-hemisphere interactions is stronger for the right. In principle, the interpretation of this metric would be complicated by the presence of negative correlations or negative contrasts. However, closer examination of the group-average values (shown in Fig. S1) reveals exclusively positive correlations for LL, LR, RR, and RL throughout the brain (69). The segregation metric and its component left- and right-sided contrasts ($LL-LR$ and $RR-RL$), also shown in Fig. S1, further demonstrate that the above interpretation is not complicated by ambiguities resulting from negative correlations/contrasts.

The second form of lateralization, referred to as integration, is calculated as a sum of average intra- and interhemispheric correlations, compared at homotopic left- and right-hemisphere nodes:

$$Integration = LL + LR - (RR + RL).$$

Large positive values of the integration metric imply stronger bilateral interactions with left-hemisphere nodes, whereas large negative values imply stronger bilateral interactions with the right. Note that this metric is similar to the single "laterality" index used in Liu et al. (16).

Multidimensional Scaling and Cluster Analyses. Having identified 10 left-lateralized regions with the segregation metric and 8 right-lateralized regions with the integration metric (Table S1), we analyzed the interrelationships among the regions, using a two-step approach. In the first step, the large differences in surface area of the different regions were handled by randomly sampling the same number of nodes ($n = 20$) from each region. On a given iteration, the nodes were randomly sampled and the corresponding time series were entered into a large matrix (20 nodes from 18 regions = 360 nodes × 136 TRs). The all-to-all node correlation matrix (360 × 360) was calculated and then submitted to cluster analyses, using the K-means algorithm (kmeans in Matlab's Statistics Toolbox, with the default Squared Euclidean Distance metric) (22). In K-means cluster analysis, a matrix is partitioned into groups or "clusters" of columns such that the variance explained by the clustering (i.e., the between-clusters sum-of-squares relative to the total sum-of-squares) is optimized (70). For choices of K ranging from 2 to 10, we tabulated the number of times that nodes sampled from one of the 18 regions were clustered together with nodes from each of the other 18 regions, and this process was repeated for a total of 100 iterations. Averaging the results across the 100 iterations, we calculated the likelihood that nodes sampled from any pair of regions were clustered together, given the choice of K (Fig. S3). "Elbow" plots of the variance left unexplained for each of the 100 iterations with increasing K (calculated as the within-cluster sum-of-squares over the relevant columns of correlation values) were combined with a measure of stability of the resulting likelihood matrix (a measure of sum-squared distance between adjacent values of K, calculated over the likelihood values in the 18 × 18 region matrix). A choice of K = 5 in this first step resulted in good variance explained and little subsequent change in the average likelihood matrix; the final clustering results (below) did not depend strongly on this particular choice (results are identical for K = 6). Chance clustering levels were determined for K = 5, using random time series (each time point drawn from a Gaussian normal distribution with $\mu = 0$ and $\sigma = 1$) and Monte Carlo methods. For each iteration of the Monte Carlo simulations (total of 20,000 iterations), (i) a set of 360 random time series (representing 18 regions × 20 nodes) of the same length as the fMRI time series (136 TRs) was correlated all-to-all to yield a 360 × 360 correlation matrix, (ii) this matrix was clustered with K-means using K = 5, (iii) the number of times each combination of the 18 "regions" was clustered together was tabulated, and (iv) steps i–iii were repeated 100 times to match the sampling process performed on the actual data. The distribution of chance likelihood values across the 20,000 iterations was then compared against the values for the actual data. Controlling for a Bonferroni-corrected chance level ($P < 0.05$ divided by the number of unique

comparisons in the 18 × 18 matrix or $P = 0.05/171 = 0.0002924$ for a two-tailed test) meant that any actual clustering likelihood values above the 99.99th percentile in the chance distributions (likelihood threshold of 0.432) would be corrected for chance anywhere in the 18 × 18 matrix. Black circles in particular cells of the 18 × 18 matrix in Fig. 3C indicate significant clustering likelihood values by these methods.

In the second step of the cluster analysis approach, the average likelihood matrix was submitted to a final round of K-means clustering (shown in Fig. 3) and multidimensional scaling (MDS) after conversion to a dissimilarity matrix (using Matlab's pdist function and then mdscale in the Statistics Toolbox with default options for parametric MDS). MDS is an analysis method that takes points in a high-dimensional space (18 dimensions, in this case) and rerepresents their interrelationships as accurately as possible in a lower-dimensional space that can be more easily visualized (71). A four-cluster solution provided the best trade-off of variance explained to model complexity according to a simple elbow criterion (the point of maximum concavity along the curve of number of clusters, K, vs. variance unexplained; see ref. 72 and Fig. 3A, Inset). Results using a five-cluster solution were identical to those using the four-cluster solution with the exception that the large left somatosensory/motor region split off on its own from the other regions outlined in green in Fig. 3. The four K-means clusters were viewed simultaneously in the plane of the MDS plot, using color (red, green, and light and dark blue) to verify the basic agreement of the two separate analysis methods (see ref. 24 for a similar application). Fig. S5 provides detailed information about the membership of regions in the four clusters, shown along with the region-by-region likelihood matrix sorted by cluster.

Permutation Tests for Correlations with Verbal and Visuospatial Ability. The joint likelihood of the family of effects observed for each of the regions reported in Figs. 4 and 5 was estimated by permutation test (34). Four partial correlation tests were carried out for each of these regions: (test 1) partial correlation of vocabulary scores with the full segregation metric for cluster 1 ROIs, partialling block design scores (or block design/matrix reasoning with integration, removing vocabulary for cluster 4 ROIs); (test 2) partial correlation of these same behavioral scores with the opposite lateralization metric; (test 3) partial correlation for the same-sided component metric (e.g., $LL-LR$ for the segregation metric in a left-hemisphere ROI); and (test 4) partial correlation for the opposite-sided component metric (e.g., $RR-RL$ for the segregation metric in a left-hemisphere ROI). The patterns observed in the actual data were (i) significant effects for tests 1 and 3, and (ii) non-significant effects for tests 2 and 4 (i.e., $P > 0.1$). To estimate the chance likelihood of these four events for each region, we randomly repaired each participant's laterality measures with a different participant's behavioral scores (20,000 times), recalculating all of the same partial correlations and tabulating the number of times that the randomized data showed effects in tests 1 and 3 at significance levels matching the weakest one observed for that region in the actual data and exhibiting P values in tests 2 and 4 greater than or equal to 0.1. We further required that the partial correlation coefficients in tests 1 and 3 exhibited the same sign, as all of the significant partial r-values for the actual data were positive. Significance of the estimated joint likelihoods was then found by comparing the percentage of the chance events observed against a Bonferroni-corrected value of $P = 0.05/16$ (the number of regions tested in the actual data: six cluster 1 ROIs and five cluster 4 ROIs tested twice each).

Interrelationships of Lateralization in Language, Motor, and Visuospatial Regions: Controlling for Whole-Brain Correlations. Whole-brain correlation was measured for each participant by calculating the average correlation of each node's time series with that at every other node on the cortical surface in both hemispheres (using AFNI's function 3dTcorrMap) and then averaging further over these node-wise average correlations to arrive at a single global correlation value. This global correlation value was then removed using linear regression from the participant-level lateralization metrics at each node in the 18 lateralized regions that were detected with either segregation or integration metrics. Despite the potential concern that whole-brain correlation could bias these analyses, results were virtually identical with or without the removal of this variable.

Gotts et al.

1. Mesulam MM (1990) Large-scale neurocognitive networks and distributed processing for attention, language, and memory. *Ann Neurol* 28(5):597–613.
2. Gazzaniga MS (1995) Principles of human brain organization derived from split-brain studies. *Neuron* 14(2):217–228.
3. Kimura D, Archibald Y (1974) Motor functions of the left hemisphere. *Brain* 97(2):337–350.
4. Springer JA, et al. (1999) Language dominance in neurologically normal and epilepsy subjects: A functional MRI study. *Brain* 122(Pt 11):2033–2046.
5. Annett M (1976) Handedness and the cerebral representation of speech. *Ann Hum Biol* 3(4):317–328.
6. Heilman KM, Van Den Abell T (1980) Right hemisphere dominance for attention: The mechanism underlying hemispheric asymmetries of inattention (neglect). *Neurology* 30(3):327–330.
7. Jacobs RA (1999) Computational studies of the development of functionally specialized neural modules. *Trends Cogn Sci* 3(1):31–38.
8. Kosslyn SM (1987) Seeing and imagining in the cerebral hemispheres: A computational approach. *Psychol Rev* 94(2):148–175.
9. Plaut DC, Behrmann M (2011) Complementary neural representations for faces and words: A computational exploration. *Cogn Neuropsychol* 28(3–4):251–275.
10. Crow TJ, Crow LR, Done DJ, Leask S (1998) Relative hand skill predicts academic ability: Global deficits at the point of hemispheric indecision. *Neuropsychologia* 36(11):1275–1282.
11. Toga AW, Thompson PM (2003) Mapping brain asymmetry. *Nat Rev Neurosci* 4(1):37–48.
12. Jo HJ, Saad ZS, Gotts SJ, Martin A, Cox RW (2012) Quantifying agreement between anatomical and functional interhemispheric correspondences in the resting brain. *PLoS ONE* 7(11):e48847.
13. Van Essen DC, Glasser MF, Dierker DL, Harwell J, Coalson T (2012) Parcellations and hemispheric asymmetries of human cerebral cortex analyzed on surface-based atlases. *Cereb Cortex* 22(10):2241–2262.
14. Seghier ML, Josse G, Leff AP, Price CJ (2011) Lateralization is predicted by reduced coupling from the left to right prefrontal cortex during semantic decisions on written words. *Cereb Cortex* 21(7):1519–1531.
15. Powell JL, Kemp GJ, García-Finaña M (2012) Association between language and spatial laterality and cognitive ability: An fMRI study. *Neuroimage* 59(2):1818–1829.
16. Liu H, Stufflebeam SM, Sepulcre J, Hedden T, Buckner RL (2009) Evidence from intrinsic activity that asymmetry of the human brain is controlled by multiple factors. *Proc Natl Acad Sci USA* 106(48):20499–20503.
17. Gee DG, et al. (2011) Low frequency fluctuations reveal integrated and segregated processing among the cerebral hemispheres. *Neuroimage* 54(1):517–527.
18. Allen M (1983) Models of hemispheric specialization. *Psychol Bull* 93(1):73–104.
19. Lackner JR, Teuber HL (1973) Alterations in auditory fusion thresholds after cerebral injury in man. *Neuropsychologia* 11(4):409–415.
20. Poeppel D (2003) The analysis of speech in different temporal integration windows: Cerebral lateralization as 'asymmetric sampling in time'. *Speech Commun* 41(1):245–255.
21. Semmes J (1968) Hemispheric specialization: A possible clue to mechanism. *Neuropsychologia* 6(1):11–26.
22. Corbetta M, Shulman GL (2011) Spatial neglect and attention networks. *Annu Rev Neurosci* 34:569–599.
23. Fox MD, Raichle ME (2007) Spontaneous fluctuations in brain activity observed with functional magnetic resonance imaging. *Nat Rev Neurosci* 8(9):700–711.
24. Gotts SJ, et al. (2012) Fractionation of social brain circuits in autism spectrum disorders. *Brain* 135(Pt 9):2711–2725.
25. Turken AU, Dronkers NF (2011) The neural architecture of the language comprehension network: Converging evidence from lesion and connectivity analyses. *Front Syst Neurosci* 5:1.
26. Adolphs R (2009) The social brain: Neural basis of social knowledge. *Annu Rev Psychol* 60:693–716.
27. Meier JD, Aflalo TN, Kastner S, Graziano MS (2008) Complex organization of human primary motor cortex: A high-resolution fMRI study. *J Neurophysiol* 100(4):1800–1812.
28. Epstein RA (2008) Parahippocampal and retrosplenial contributions to human spatial navigation. *Trends Cogn Sci* 12(10):388–396.
29. Martin A (2007) The representation of object concepts in the brain. *Annu Rev Psychol* 58:25–45.
30. Seidel WT (1994) Applicability of the hooper visual organization test to pediatric populations: Preliminary findings. *Clin Neuropsychol* 8(1):59–68.
31. Semel E, Wiig EH, Secord W (2003) *Clinical Evaluation of Language Fundamentals (CELF-4)* (Psychological Corp, San Antonio) 4th Ed.
32. Trahan DE (1998) Judgment of line orientation in patients with unilateral cerebro-vascular lesions. *Assessment* 5(3):227–235.
33. Warrington EK, James M, Maciejewski C (1986) The WAIS as a lateralizing and localizing diagnostic instrument: A study of 656 patients with unilateral cerebral lesions. *Neuropsychologia* 24(2):223–239.
34. Maris E, Oostenveld R (2007) Nonparametric statistical testing of EEG- and MEG-data. *J Neurosci Methods* 164(1):177–190.
35. Levy J (1969) Possible basis for the evolution of lateral specialization of the human brain. *Nature* 224(5219):614–615.
36. Cai Q, Van der Haegen L, Brysbaert M (2013) Complementary hemispheric specialization for language production and visuospatial attention. *Proc Natl Acad Sci USA* 110(4):E322–E330.
37. Rosch RE, Bishop DV, Badcock NA (2012) Lateralised visual attention is unrelated to language lateralisation, and not influenced by task difficulty - a functional transcranial Doppler study. *Neuropsychologia* 50(5):810–815.
38. Damasio AR, Geschwind N (1984) The neural basis of language. *Annu Rev Neurosci* 7:127–147.
39. Binder JR, Desai RH, Graves WW, Conant LL (2009) Where is the semantic system? A critical review and meta-analysis of 120 functional neuroimaging studies. *Cereb Cortex* 19(12):2767–2796.
40. Yeo BT, et al. (2011) The organization of the human cerebral cortex estimated by intrinsic functional connectivity. *J Neurophysiol* 106(3):1125–1165.
41. Kravitz DJ, Saleem KS, Baker CI, Mishkin M (2011) A new neural framework for visuospatial processing. *Nat Rev Neurosci* 12(4):217–230.
42. Yousry TA, et al. (1997) Localization of the motor hand area to a knob on the precentral gyrus. A new landmark. *Brain* 120(Pt 1):141–157.
43. Honey CJ, et al. (2009) Predicting human resting-state functional connectivity from structural connectivity. *Proc Natl Acad Sci USA* 106(6):2035–2040.
44. Wang Z, et al. (2013) The relationship of anatomical and functional connectivity to resting-state connectivity in primate somatosensory cortex. *Neuron* 78(6):1116–1126.
45. Fransson P, et al. (2007) Resting-state networks in the infant brain. *Proc Natl Acad Sci USA* 104(39):15531–15536.
46. Vincent JL, et al. (2007) Intrinsic functional architecture in the anaesthetized monkey brain. *Nature* 447(7140):83–86.
47. Carroll JB (1993) *Human Cognitive Abilities* (Cambridge Univ Press, Cambridge, UK).
48. Burton DB, Ryan JJ, Axelrod BN, Schellenberger T (2002) A confirmatory factor analysis of the WAIS-III in a clinical sample with crossvalidation in the standardization sample. *Arch Clin Neuropsychol* 17(4):371–387.
49. Holdnack JA, Xiaobin Zhou, Larrabee GJ, Millis SR, Salthouse TA (2011) Confirmatory factor analysis of the WAIS-IV/WMS-IV. *Assessment* 18(2):178–191.
50. Ryan JJ, et al. (2003) Exploratory factor analysis of the Wechsler Abbreviated Scale of Intelligence (WASI) in adult standardization and clinical samples. *Appl Neuropsychol* 10(4):252–256.
51. Ungerleider LG, Mishkin M (1982) *Analysis of Visual Behavior*, eds Ingle DJ, Goodale MA, Masfield RJW (MIT Press, Cambridge, MA), pp 549–586.
52. Hickok G, Poeppel D (2007) The cortical organization of speech processing. *Nat Rev Neurosci* 8(5):393–402.
53. Doron KW, Bassett DS, Gazzaniga MS (2012) Dynamic network structure of interhemispheric coordination. *Proc Natl Acad Sci USA* 109(46):18661–18668.
54. Denckla MB (1985) Revised neurological examination for subtle signs (1985). *Psychopharmacol Bull* 21(4):773–800.
55. Wechsler D (1999) *Wechsler Abbreviated Scale of Intelligence* (The Psychological Corp, San Antonio).
56. Wechsler D (1981) *Adult Intelligence Scale-Revised* (The Psychological Corp, San Antonio).
57. Wallace GL, et al. (2010) A bivariate twin study of regional brain volumes and verbal and nonverbal intellectual skills during childhood and adolescence. *Behav Genet* 40(2):125–134.
58. Wallace GL, et al. (2013) Increased gyrification, but comparable surface area in adolescents with autism spectrum disorders. *Brain* 136(Pt 6):1956–1967.
59. Colom R, Jung RE, Haier RJ (2006) Distributed brain sites for the g-factor of intelligence. *Neuroimage* 31(3):1359–1365.
60. Power JD, Barnes KA, Snyder AZ, Schlaggar BL, Petersen SE (2012) Spurious but systematic correlations in functional connectivity MRI networks arise from subject motion. *Neuroimage* 59(3):2142–2154.
61. Fischl B, et al. (2002) Whole brain segmentation: Automated labeling of neuro-anatomical structures in the human brain. *Neuron* 33(3):341–355.
62. Cox RW (1996) AFNI: Software for analysis and visualization of functional magnetic resonance neuroimages. *Comput Biomed Res* 29(3):162–173.
63. Argall BD, Saad ZS, Beauchamp MS (2006) Simplified intersubject averaging on the cortical surface using SUMA. *Hum Brain Mapp* 27(1):14–27.
64. Saad ZS, Reynolds RC, Argall RC, Japee S, Cox RW (2004) SUMA: An interface for surface-based intra- and inter-subject analysis with AFNI. *Proceedings of the 2004 International Symposium on Biomedical Imaging* (Institute of Electrical and Electronic Engineers, Arlington, VA), pp 1510–1513.
65. Jo HJ, Saad ZS, Simmons WK, Milbury LA, Cox RW (2010) Mapping sources of correlation in resting state FMRI, with artifact detection and removal. *Neuroimage* 52(2):571–582.
66. Glover GH, Li TQ, Ress D (2000) Image-based method for retrospective correction of physiological motion effects in fMRI: RETROICOR. *Magn Reson Med* 44(1):162–167.
67. Birn RM, Smith MA, Jones TB, Bandettini PA (2008) The respiration response function: The temporal dynamics of fMRI signal fluctuations related to changes in respiration. *Neuroimage* 40(2):644–654.
68. Fox MD, et al. (2005) The human brain is intrinsically organized into dynamic, anticorrelated functional networks. *Proc Natl Acad Sci USA* 102(27):9673–9678.
69. Murphy K, Birn RM, Handwerker DA, Jones TB, Bandettini PA (2009) The impact of global signal regression on resting state correlations: Are anti-correlated networks introduced? *Neuroimage* 44(3):893–905.
70. Lloyd S (1982) Least squares quantization in PCM. *IEEE Trans Inf Theory* 28(2):129–137.
71. Cox TF, Cox MAA (2001) *Multidimensional Scaling* (Chapman & Hall/CRC Press, Boca Raton, FL).
72. Thorndike R (1953) Who belongs in the family? *Psychometrika* 18(4):267–276.

www.manaraa.com